Click Here for Full Article

Breaking up the hanging wall of a rift-border fault: The 2009 Karonga earthquakes, Malawi

J. Biggs,[1] E. Nissen,[2] T. Craig,[2] J. Jackson,[2] and D. P. Robinson[1]

Received 11 March 2010; revised 28 April 2010; accepted 30 April 2010; published 12 June 2010.

[1] The southern East African Rift has an unusually large seismogenic thickness (35–40 km), which is responsible for wide tilted basins and extremely long faults with the potential for M7-8 normal-faulting earthquakes. From 6–19 December 2009, a shallow earthquake sequence (four of $M_w > 5.5$) hit the Karonga region of northern Lake Malawi. The location is 50 km west of the rift-bounding Livingstone Fault, within the hanging-wall. We used seismology and InSAR to obtain source parameters and combined this with information on rift structure from geomorphology and seismic profiles. The deformation is consistent with rupture of a shallow, west-dipping fault, with no evidence for the involvement of magmatic fluids. Although the Livingstone Fault dominates local geomorphology, the Karonga earthquakes demonstrate that the hanging-wall block is actively breaking up, reflecting temporal and spatial migration of activity or the release of stresses within it. **Citation:** Biggs, J., E. Nissen, T. Craig, J. Jackson, and D. P. Robinson (2010), Breaking up the hanging wall of a rift-border fault: The 2009 Karonga earthquakes, Malawi, *Geophys. Res. Lett.*, *37*, L11305, doi:10.1029/2010GL043179.

1. Introduction

[2] Between 6th and 19th December 2009, a sequence of earthquakes hit the Karonga region of Malawi. Four had magnitudes of $M_w > 5.5$, and five further events had M_b 5.0–5.2. Over 1000 houses collapsed, a further 2900 were damaged, 300 people were wounded, and 4 were killed [*Office of the United Nations Resident Coordinator*, 2009]. The prolonged duration of seismicity resulted in the evacuation of over 5000 families and the Malawi Government declared Karonga a National Disaster Area on 21st December. The large-scale features, clear geomorphology and seismic profiling of sub-surface structures characterise the rift structure in this region. The 2009 Karonga earthquakes are among the first to be studied with InSAR in the East African Rift and provide an excellent opportunity to study active normal faulting within this setting.

1.1. Geological Background

[3] The Malawi Rift lies in the southern part of East African Rift System (EARS) where GPS-derived model extension rates are 3.7–3.8 mm/yr [*Stamps et al.*, 2008]. The 60 km wide Karonga Basin lies at the northern end of Lake Malawi (Figure 1a). The rift boundary fault (the 120-km-long Livingstone Fault) forms a 2-km-high escarpment on the eastern shore. The Karonga Basin is strongly asymmetric with water depths and sediment thicknesses greatest adjacent to the Livingstone Fault [*Flannery and Rosendahl*, 1990] indicating a total throw of ~6 km [*Ebinger et al.*, 1999]. Within the lake, seismic reflection profiles show a series of sub-parallel, W-dipping faults [*Flannery and Rosendahl*, 1990].

[4] In contrast to the steep eastern boundary, the western shore comprises a 5–10 km-wide coastal plain covered by Quaternary sediments (Figures 1b and 1c). Further west, hilly topography composed of Precambrian bedrock rises along the E-dipping Karonga Fault (Figures 1b and 1c). The surface expression of the Karonga Fault is clear north of Karonga but is obscured to the south by a number of discontinuous W-dipping faults, before resuming again near Chilumba (Figures 1b and 1c).

[5] The Pan-African erosional surface, the result of continental denudation from 160Ma to 30 Ma [*Burke and Gunnell*, 2008], dips gently eastwards in the hills west of Karonga. The absence of westward back-tilting associated with the Karonga Fault points to the dominant influence of the Livingstone Fault (~50 km to the NE). Across the Karonga Fault, this erosion surface is displaced vertically by ~650 m assuming an equivalent sedimentary thickness (400m) to that estimated by seismic profiles under the lake [*Flannery and Rosendahl*, 1990].

2. Observations and Modelling

2.1. Seismology

[6] For the largest 4 earthquakes (the 6th, 8th, 12th and 19th December), we modelled teleseismic P and SH waveforms using the methods of *Foster and Jackson* [1998] (Table 1 and Figures 1b and S2–S5 of the auxiliary material).[3] All four E-dipping nodal planes have similar strikes (150–170°), dips (~40°) and rakes (within 25° of pure normal). Centroid depths are well constrained to <8 km, with formal misfit minima of 4–6 km. The 8th December event has a slightly different orientation, but is also the least well constrained by station distribution and quality. The rupture dimensions (Table 1) were estimated from scaling relations, assuming equidimensional rupture and a slip-to-length ratio of 5×10^{-5} [*Scholz*, 1990].

[7] The Quick Global CMT epicenters are aligned NNW-SSE (Figure 1b), consistent with the fault strike, but errors in absolute location are larger than the distances between events. We manually re-picked the P-wave first arrivals for

[1]NCEO, Department of Earth Sciences, University of Oxford, Oxford, UK.
[2]NCEO, Department of Earth Sciences, University of Cambridge, Cambridge, UK.

Copyright 2010 by the American Geophysical Union.
0094-8276/10/2010GL043179

[3]Auxiliary materials are available in the HTML. doi:10.1029/2010GL043179.

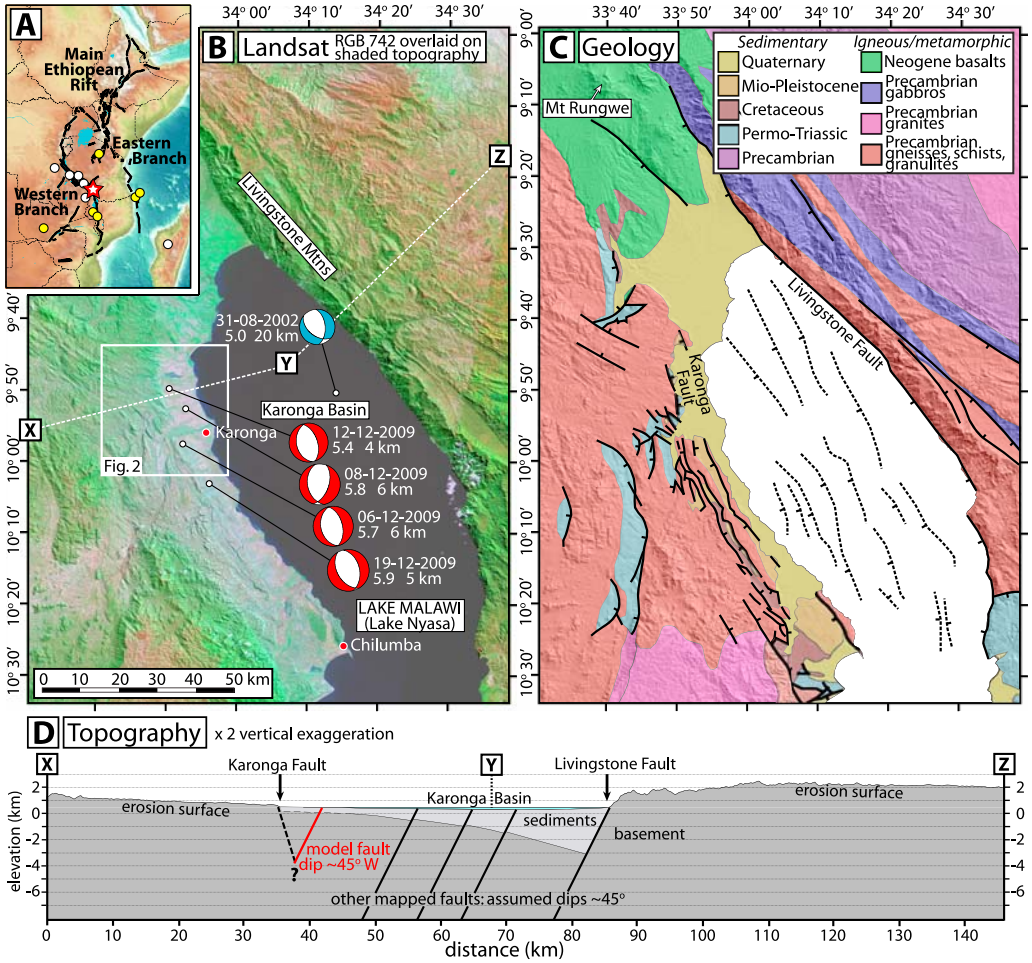

Figure 1. (a) Major faults of the East African Rift System. Red star marks the Karonga region. Circles are earthquakes with centroid depths of 20–30 km (white) and 30–40 km (yellow), from *Foster and Jackson* [1998]. (b) Landsat image of northern Lake Malawi with focal mechanisms of the Karonga earthquakes and the 2002 event plotted with dates, moment magnitudes and centroid depths, at Quick CMT locations. X-Y-Z marks the cross-section in Figure 1d. (c) Geological map modified from *Geological Survey of Tanzania* [1959] and *Geological Survey of Malawi* [1966]. Faults are denoted by thick black lines; those under Lake Malawi (dashed) are from *Mortimer et al.* [2007]. (d) Cross-section showing major active faults and sediment thickness [from *Mortimer et al.*, 2007].

each earthquake from seismic recordings at the closest stations. Differences in travel times to stations to the north and south reflect the relative position of each earthquake along the fault (Figure S6). This confirms the sequence of events from north to south to be 12/12/09, 08/12/09, 06/12/09, 19/12/09, as reported by GCMT (Figure S6).

[8] The only other event in the Global CMT catalogue for the region was a M_w 5.0 earthquake in 2002. Modelling this event, we found a normal-faulting mechanism with a depth of 20 km (Table 1 and Figures 1b and S1). The orientation and location are consistent with rupture of a small patch of the Livingstone Fault, and the depth is consistent with those of earthquakes in S Malawi, S Tanzania and NE Zambia [*Foster and Jackson*, 1998; *Jackson and Blenkinsop*, 1993].

2.2. InSAR

[9] The European Space Agency (ESA) provided Envisat data from several tracks and look vectors. We used archived images from May 2009 in beam mode D2 and D5, from September in A4 and early December in A3. Due to a swift response, an image was collected in beam mode A2 on

Table 1. Parameters From Body Wave and InSAR Uniform Slip Models[a]

	Body-Wave				InSAR Uniform Slip	
	6-Dec	8-Dec	12-Dec	19-Dec	All	19-Dec
Strike	167	168	169	150	164	155
Dip	38	40	37	46	41	41
Rake	272	245	277	258	275	268
Long	33.87	33.88	33.84	33.93	33.89	33.90
Lat	−9.96	−9.88	−9.83	−10.05	−9.88	−9.89
Length[b]	6.3	7.4	5.3	8.3	17.8	14.0
Centroid–[b]	6	6	4	5	-	-
Top Depth[b]	4.0	4.0	2.7	3.4	0	0
BottomDepth[b]	8	8	5.3	6.6	5.8	6.4
Slip[c]	0.3	0.4	0.3	0.4	0.8	0.4
Moment[d]	3.8	6.2	2.3	8.7	32.2	14.0
M_w	5.7	5.8	5.5	5.9	6.3	6.0

[a]The InSAR model "All" uses the interferograms in Figures 2b and 2c and "19-Dec" uses the interferogam in Figure 2a. Body-wave locations are from the Quick CMT catalog.
[b](km).
[c](m).
[d](Nm × 10^{17}).

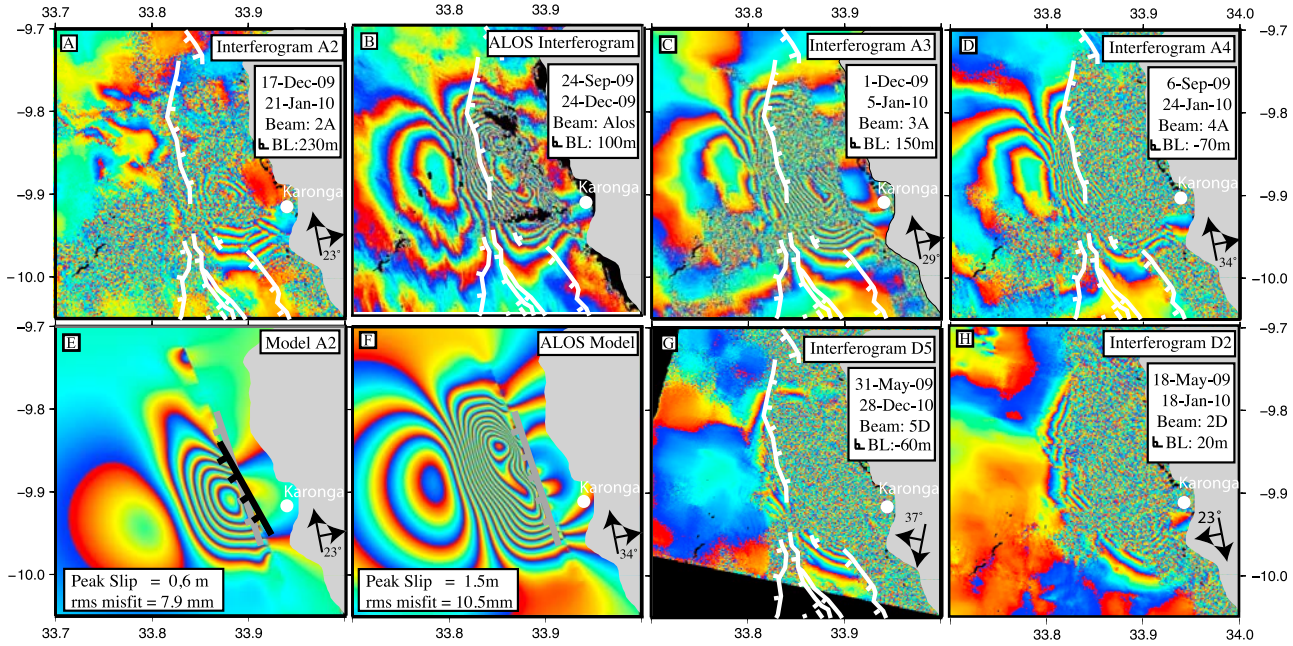

Figure 2. Envisat Interferograms for the 2009 Karonga earthquakes, Malawi. Interferogram (a) A2 covers only the December 19th event; interferograms (b) Alos, (c) A3, (d) A4, (g) D5, and (h) D2 cover the entire sequence. Distributed slip models shown for (e) A2 and (f) Alos. The grey line is the surface projection of the best fitting uniform slip model for all events and the black line for the 19 December event. White lines are mapped faults.

December 17th allowing us to isolate the deformation from the 19th December earthquake (Figure 2c). The coastal plain lost interferometric coherence within a few months but bedrock west of the Karonga fault maintained coherence (Figure 2). We produce one interferogram using images in September and December 2009 from the Japanese satellite ALOS. Due to the longer wavelength radar, this interferogram is more coherent along the vegetated shore.

[10] Interferograms spanning the whole sequence show three parallel deformation lobes, elongated NNW-SSE (Figure 2). The largest displacements occur in the central lobe (28 cm range increase) with smaller amounts of range decrease in the western and eastern lobes. A sharp discontinuity between the central and eastern lobes lies on the coastal plain, while the smoother boundary between the western and central lobes lies 2–3 km west of the Karonga fault-scarp (Figure 3). The western lobe contains more fringes in the E-looking ascending interferograms than in the W-looking descending ones, consistent with mostly westward displacements. The interferogram covering the 19th December earthquake shows a simpler bulls eye pattern of 4 fringes, with the same discontinuity in the coastal plain (Figure 2c).

[11] We applied a non-linear inversion to find the best-fitting uniform slip on a single, rectangular fault plane [*Okada*, 1985; *Wright et al.*, 1999; *Biggs et al.*, 2009b]. Only the more-coherent A3 and A4 interferograms were used in the modelling. Fixing the geometry, we then used a smoothed, non-negative linear inversion to estimate the distributed slip pattern [*Funning et al.*, 2007].

[12] A single W-dipping fault plane is sufficient to fit all interferograms well. The model geometry is compatible with seismological estimates for the W-dipping plane, and slip is confined to the top 6 km. Although no surface rupture has yet been reported, numerous photographs of ground cracks and fissures suggest the rupture either broke or came close to the surface, consistent with this model. Forward models

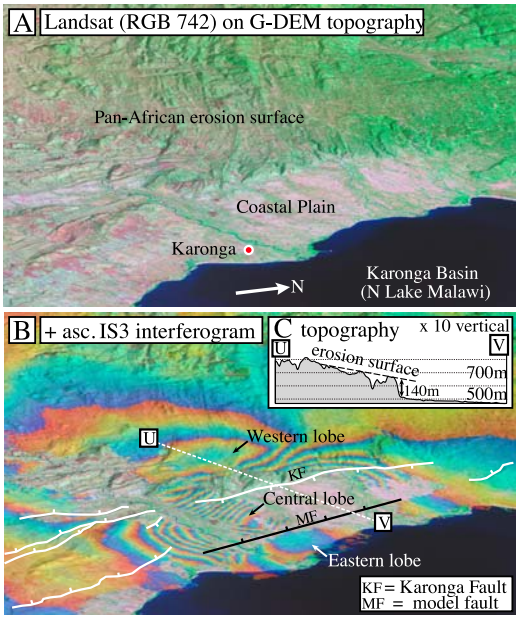

Figure 3. (a) Perspective view of the Karonga region. (b) A3 interferogram draped over Figure 3a, with geological faults in white and the model fault in black. (c) Cross-section showing the E-dipping erosion surface in the footwall of the Karonga fault.

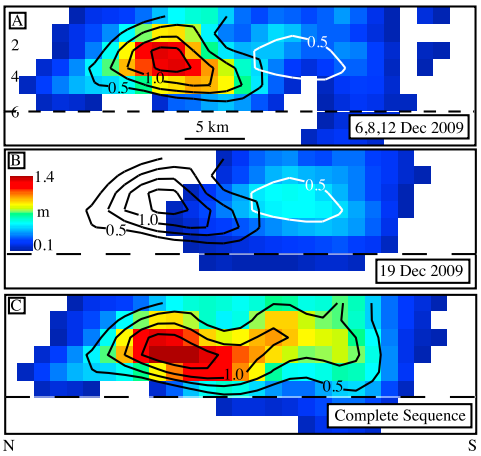

Figure 4. Slip distributions showing a southward shift between events on 6–12 December and the 19th December earthquake. Slip distribution B corresponds to model A2 (Figure 2g); distribution C corresponds to Alos model (Figure 2f).

based on body-wave solutions suggest that each of the M > 5.5 earthquakes contributes at least 2 fringes. The best uniform slip model matches the bullseye pattern caused by the deep slip does not break the surface so cannot reproduce the observed discontinuity. The eastern lobe corresponds to footwall uplift and the smooth boundary between the western and central lobes reflects the base of the fault. The event on the 19th has a lower strike in both body wave and InSAR models, suggesting a slight curvature in the fault.

[13] We tested E-dipping model faults but these project to the surface at the boundary between the western and central lobes, 2–3 km west of the Karonga Fault scarp (Figure S6). Furthermore, these models cannot reproduce the discontinuity between the central and eastern lobes.

[14] A distributed slip model is required to match both the magnitude of slip at depth and the discontinuity caused by fault slip at the surface. We used a single fault with a strike of 160°, dip of 41° and rake of 270°. The model for the 19th December earthquake has a peak slip of 0.63 m compared to 1.46 m for the whole sequence (Figure 4). RMS misfits are 8.6 and 10.5 mm respectively with the largest residuals located close to the fault break (Figure S7). The rupture dimensions are consistent with those estimated from seismology, although the InSAR-derived depths are shallower by ~2 km.

[15] Subtracting these models gives the slip for the 6–12th December earthquakes. There is a southward progression between the first three events (6, 8, 12 Dec) and the final event (19 Dec) consistent with the relative locations from P-wave arrivals. There is no overlap of slip patches above the 50 cm contour (Figure 4). Rather than one M_w 6.3 earthquake, slip occurred in a sequence of four M_w 5.5–6 events over two weeks. This suggests an irregular fault geometry, with breaks caused by small step-overs or changes in strike, consistent with an immature fault with little geomorphological expression.

[16] The geodetic moment (3.2×10^{18} Nm) is 1.35 times larger than the combined seismological moment of the nine events Mb > 5.0 (2.4×10^{18}), within the range of observed ratios for earthquakes in non-magmatic settings [*Elliott*, 2010]. For dike intrusions, the geodetic moment is usually 2–10 times larger than the seismological moment [*Wright et al.*, 2006; *Biggs et al.*, 2009b] so the discrepancy at Karonga does not require a magmatic contribution.

3. Discussion

[17] The southern East African Rift is characterised by an unusually large seismogenic thickness (35–40 km) which has produced wide basins and extremely long faults [*Jackson*, 1989; *Scholz and Contreras*, 1998; *Jackson*, 2001]. In most regions of continental extension, maximum graben widths are <20 km, fault lengths are <25 km and earthquakes are restricted to depths <15 km [e.g., *Jackson*, 1989; *Goldsworthy and Jackson*, 2001]. In contrast, the tilting associated with the Kargona basin extends over 50 km from the 120 km long Livingstone Fault.

[18] Magmatism and dike intrusion are important components of continental rifting even in immature sections of the EARS [*Wright et al.*, 2006; *Calais et al.*, 2008; *Biggs et al.*, 2009a; *Biggs et al.*, 2009b]. The Karonga earthquakes occurred 50 km south of Rungwe volcanic zone and do not follow a simple mainshock-aftershock pattern. Without access to local recordings, it is not possible to determine whether the larger earthquakes were accompanied by the several hundred microearthquakes a day which would characterise a swarm. However, the geodetic observations do not support the involvement of fluids or aseismic slip which this might imply. We prefer to interpret this as a sequence of earthquakes consistent with segmented faulting along strike. Similar sequences consisting of 3 or more events with similar magnitudes, are not uncommon in the earthquake catalogue (e.g., Corinth, 1981 [*Jackson et al.*, 1982]; Friuli, 1976 [*Cipar*, 1980]).

[19] The large fault dimensions in this part of the EARS hint at the potential for M7-8 earthquakes. Examples include a single-earthquake offset of 10 m on the 125 km long Bilila-Mtakataka Fault [*Jackson and Blenkinsop*, 1997], and the 1910 Rukwa Earthquake (M7.4) which occurred on the 180 km-long Kanda Fault [*Ambraseys*, 1997; *Vittori et al.*, 1997]. If the whole 120 km length of the Livingstone Fault were to rupture in a single event, scaling relations suggest a moment magnitude of ~8. However, given the low extension rates such large earthquakes are expected to be rare.

[20] Tilting of the Karonga basin extends over 50 km, consistent with the Livingstone Fault extending to the base of the crust at 40km. Yet the Karonga block is not entirely intact. It is cut by the antithetic Karonga Fault and a series of west-dipping synthetic faults, one of which ruptured during the 2009 Karonga earthquakes. This indicates that the hanging-wall of the Livingstone Fault is actively breaking up.

[21] The implications of the Karonga earthquakes for the Livingstone Fault depend on whether they reflect temporal and spatial migration of activity into the hanging wall or release of stresses within it. *Scholz and Contreras* [1998] suggested that when some limiting offset is reached, motion on the border fault will cease, and a new fault will develop. A similar pattern occurs in Greece, where faulting has migrated into the hanging walls [*Goldsworthy and Jackson*, 2001]. However, a simpler explanation is that

both systems are active simultaneously, with smaller faults in the hanging wall driven by stresses that arise from the lateral density contrasts between the basin and its footwall [*Foster and Nimmo*, 1996].

[22] As the Karonga earthquake sequence highlights, even relatively small events can cause significant damage. Slip in the 2009 earthquakes was confined to the upper 6 km, but in this area the seismogenic layer is ~35 km thick [*Foster and Jackson*, 1998; *Ebinger et al.*, 1999]. The depth extent of this and other mapped structures are key to understanding the interactions of faults at depth, but are currently poorly known. The lower 30 km of the seismogenic layer may have been loaded by the Karonga earthquakes and if this were to rupture seismically, the earthquake would have a correspondingly larger magnitude.

[23] **Acknowledgments.** JB was supported by the ESA Changing Earth Science Network, EN by the National Centre for Earth Observation Dynamic Earth Theme and DPR by NERC grant NE/D004381/1 We thank ESA for access to their archive of Envisat images, and their quick response in scheduling new acquisitions and the IRIS Data Management Centre. We thank Donna Shillington and one anonymous reviewer for their helpful comments.

References

Ambraseys, N. (1997), The Rukwa earthquake of 13 December 1910 in East Africa, *Terra Nova*, *3*, 202–211.

Biggs, J., F. Amelung, N. Gourmelen, T. H. Dixon, and S. Kim (2009a), InSAR observations of 2007 Tanzania rifting episode reveal mixed fault and dyke extension in an immature continental rift, *Geophys. J. Int.*, *179*, 549–558, doi:10.1111/j.1365-246X.2009.04262.x.

Biggs, J., E. Anthony, and C. Ebinger (2009b), Multiple inflation and deflation events at Kenyan volcanoes, East African Rift, *Geology*, *37*, 979–982, doi:10.1130/G30133A.1.

Burke, K., and Y. Gunnell (2008), *The African Erosion Surface: A Continental-Scale Synthesis of Geomorphology, Tectonics, and Environmental Change Over the Past 180 Million Years*, *Geol. Soc. Am. Mem.*, 201, 66 pp., doi:10.1130/2008.1201.

Calais, E., et al. (2008), Strain accommodation by slow slip and dyking in a youthful continental rift, East Africa, *Nature*, *456*, 783–787, doi:10.1038/nature07478.

Cipar, J. (1980), Teleseismic observations of the 1976 Friuli, Italy earthquake sequence, *Bull. Seismol. Soc. Am.*, *70*, 963–983.

Ebinger, C. J., J. A. Jackson, A. N. Foster, and N. J. Hayward (1999), Extensional basin geometry and the elastic lithosphere, *Philos. Trans. R. Soc. A*, *357*, 741–765.

Elliott, J. (2010), Strain accumulation and release on the Tibetan Plateau measured using InSAR, Ph.D. thesis, Univ. of Oxford, Oxford, U. K.

Flannery, J., and B. Rosendahl (1990), The seismic stratigraphy of Lake Malawi, Africa: Implications for interpreting geological processes in lacustrine rifts, *J. Afr. Earth Sci.*, *10*(3), 519–548, doi:10.1016/0899-5362(90)90104-M.

Foster, A. N., and J. A. Jackson (1998), Source paramters of large African earthquakes: Implications for crustal rheology and regional kinematics, *Geophys. J. Int.*, *134*, 422–448.

Foster, A., and F. Nimmo (1996), Comparisons between the rift systems of East Africa, Earth and Beta Regio, Venus, *Earth Planet. Sci. Lett.*, *143*, 183–195, doi:10.1016/0012-821X(96)00146-X.

Funning, G. J., B. Parsons, and T. J. Wright (2007), Fault slip in the 1997 Manyi, Tibet earthquake from linear elastic modelling of InSAR displacements, *Geophys. J. Int.*, *169*, 988–1008, doi:10.1111/j.1365-246X.2006.03318.x.

Geological Survey of Malawi (1966), Geological map of Malawi, scale 1/1,000,000, Geol. Surv. of Malawi, Lilongwe.

Geological Survey of Tanzania (1959), Geological map of Tanganyika, scale 1/2,000,000, Geol. Surv. of Tanzania, Dodoma.

Goldsworthy, M., and J. Jackson (2001), Migration of activity within normal fault systems: Examples from the Quaternary of mainland Greece, *J. Struct. Geol.*, *23*, 489–506, doi:10.1016/S0191-8141(00)00121-8.

Jackson, J. (1989), Normal faulting in the upper continental crust: Observations from regions of active extension, *J. Struct. Geol.*, *11*, 15–36, doi:10.1016/0191-8141(89)90033-3.

Jackson, J. (2001), Living with earthquakes: Know your faults, *J. Earthquake Eng.*, *5*, 5–123, doi:10.1080/13632460109350530.

Jackson, J., and T. Blenkinsop (1993), The Malaŵi earthquake of March 10, 1989: Deep faulting within the East African Rift system, *Tectonics*, *12*, 1131–1139, doi:10.1029/93TC01064.

Jackson, J., and T. Blenkinsop (1997), The Bilila-Mtakataka fault in Malaŵi: An active, 100-km long, normal fault segment in thick seismogenic crust, *Tectonics*, *16*, 137–150, doi:10.1029/96TC02494.

Jackson, J. A., J. Gagnepain, G. Houseman, G. C. P. King, P. Papadimitriou, C. Soufleris, and J. Virieux (1982), Seismicity, normal faulting, and the geomorphological development of the Gulf of Corinth (Greece): The Corinth earthquakes of February and March 1981, *Earth Planet. Sci. Lett.*, *57*, 377–397, doi:10.1016/0012-821X(82)90158-3.

Mortimer, E., D. A. Paton, C. A. Scholz, M. R. Strecker, and P. Blisniuk (2007), Orthogonal to oblique rifting: Effect of rift basin orientation in the evolution of the North basin, Malawi Rift, East Africa, *Basin Res.*, *19*, 393–407.

Office of the United Nations Resident Coordinator (2009), Malawi-Karonga earthquake situation report III, U. N., Lilongwe.

Okada, Y. (1985), Surface deformation due to shear and tensile faults in a half-space, *Bull. Seismol. Soc. Am.*, *75*, 1135–1154.

Scholz, C. (1990), *The Mechanics of Earthquakes and Faulting*, Cambridge Univ. Press, Cambridge, U. K.

Scholz, C. H., and J. C. Contreras (1998), Mechanics of continental rift architecture, *Geology*, *26*, 967–970, doi:10.1130/0091-7613(1998)026<0967:MOCRA>2.3.CO;2.

Stamps, D. S., E. Calais, E. Saria, C. Hartnady, J.-M. Nocquet, C. J. Ebinger, and R. M. Fernandes (2008), A kinematic model for the East African Rift, *Geophys. Res. Lett.*, *35*, L05304, doi:10.1029/2007GL032781.

Vittori, E., D. Delvaux, and F. Kervyn (1997), Kanda fault: A major seismogenic element west of the Rukwa Rift (Tanzania, East Africa), *J. Geodyn.*, *24*, 139–153, doi:10.1016/S0264-3707(96)00038-5.

Wright, T., B. Parsons, J. Jackson, M. Haynes, E. Fielding, P. England, and P. Clarke (1999), Source parameters of the 1 October 1995 Dinar (Turkey) earthquake from SAR interferometry and seismic bodywave modelling, *Earth Planet. Sci. Lett.*, *172*, 23–37.

Wright, T., C. Ebinger, J. Biggs, A. Ayele, G. Yirgu, D. Keir, and A. Stork (2006), Magma-maintained rift segmentation at continental rupture in the 2005 Afar dyking episode, *Nature*, *442*, 291–294.

J. Biggs and D. P. Robinson, NCEO, Department of Earth Sciences, University of Oxford, Parks Road, Oxford OX1 3PR, UK. (julietb@earth.ox.ac.uk)

T. Craig, J. Jackson, and E. Nissen, NCEO, Department of Earth Sciences, University of Cambridge, Madingley Road, Cambridge CB3 0EZ, UK.